

Gate-Tunable Superconducting Spin Valve in a van der Waals Ferromagnet/Superconductor/Ferromagnet Trilayer

A. S. Ianovskaia,¹ G. A. Bobkov,¹ A. M. Bobkov,¹ and I.V. Bobkova^{1,2}

¹*Moscow Institute of Physics and Technology, Dolgoprudny, 141700 Moscow region, Russia*

²*National Research University Higher School of Economics, 101000 Moscow, Russia*

We theoretically demonstrate a gate-tunable superconducting spin valve effect (SVE) in a van der Waals (vdW) heterostructure composed of a monolayer superconductor (S) sandwiched between two ferromagnetic (F) monolayers (F/S/F). By electrostatically gating the ferromagnetic layers to modulate their chemical potentials, the system can be continuously tuned between the *standard*, *inverse* and *triplet* (non-monotonic) SVE regimes within the same device. This tunability originates from the gate-controlled hybridization between the superconducting and ferromagnetic electronic spectra, which determines the effective exchange field induced in the S-layer. Furthermore, we reveal that gating enables exotic, non-BCS temperature dependencies of the superconducting order parameter, including reentrant superconductivity, bistable states, first-order phase transitions, and the emergence of superconductivity at finite temperatures. Our results establish vdW F/S/F trilayers as a versatile and highly controllable platform for superconducting spintronics, where external gate voltages can selectively activate different spin-valve functionalities and unconventional superconducting states.

I. INTRODUCTION

Superconductor/ferromagnet (S/F) heterostructures are a subject of intense research in superconducting spintronics, primarily driven by the unique proximity effects that emerge at their nanoscale interfaces [1–4]. One of key device concepts in this field is the superconducting spin valve, which can be implemented in both F/S/F and F/F/S geometries. Its operating principle hinges on the spin-valve effect (SVE), where the superconducting critical temperature T_c is controlled by the relative orientation of the magnetizations in the ferromagnetic layers.

In its simplest form, the SVE can be qualitatively explained as follows. In a thin-film S/F bilayer, the magnetic proximity effect induces an effective exchange field in the superconductor, which suppresses superconductivity [5, 6]. Here, “thin-film” refers to a superconducting layer thickness d_S smaller than the superconducting coherence length ξ_S , although d_S and ξ_S may extend to hundreds of monolayers. In an F/S/F trilayer, both ferromagnets induce exchange fields in the superconducting interlayer. These fields add up in the parallel (P) magnetization configuration, but partially compensate each other in the antiparallel (AP) configuration. Consequently, superconductivity is more strongly suppressed in the parallel case, resulting in $T_c^P < T_c^{AP}$ —the so-called *standard* spin-valve effect [7].

Most theoretical studies predict the standard SVE in thin-film F/S/F and F/F/S heterostructures, both in the diffusive [8–15] and ballistic [10, 16–18] transport regimes. Nevertheless, it has been theoretically predicted that the proximity effect in a ballistic thin-film F/S/F structure can also give rise to the inverse SVE [14]. In such systems, the critical temperature difference $T_c^P - T_c^{AP}$ oscillates as a function of the thickness of one ferromagnetic layer, leading to alternating regions where the standard or inverse effect is dominant. These oscillations stem from the characteristic oscillatory decay of the

Cooper pair wave function within a ferromagnetic metal [1]. Significantly, this oscillatory behavior vanishes in the diffusive limit, where Usadel equations consistently yield only the standard SVE [14]. Complementary theoretical work by Fominov *et al.* [19] demonstrated that both standard and inverse SVE manifestations in F1/F2/S systems emerge from constructive or destructive interference of Cooper pairs at the F1/F2 and F2/S interfaces.

On the experimental side, the standard SVE has been widely observed [13, 20–35]. Nonetheless, a number of studies have reported clear signatures of the *inverse* SVE, where $T_c^P > T_c^{AP}$ [33, 35–44]. It is important to note that the physical origins proposed for these experimental observations are not always rooted in the proximity effect. For instance, the inverse SVE was attributed to quasiparticle accumulation in the superconducting layer for the antiparallel configuration in Refs. [36, 38], while Refs. [37, 39, 41] ascribed it to the influence of magnetic stray fields arising from domain walls in the ferromagnets.

Beyond the standard and inverse SVE, the dependence of T_c on the misorientation angle θ can be nonmonotonic, with a minimum near $\theta = \pi/2$ [14, 19, 45–51]. This behavior is due to the generation of equal-spin triplet pairs, which correspond to long-range triplet correlations inside the ferromagnets. These pairs open an additional channel for superconductivity suppression in non-collinear magnetization configurations. Since the triplet correlations are proportional to the cross product of the two magnetizations, they are most efficiently generated near $\theta = \pi/2$, leading to a characteristic minimum in the $T_c(\theta)$ dependence.

In addition to the well-studied thin-film structures, systems comprising a few monolayers—fabricated from van der Waals (vdW) materials [52, 53]—have emerged as promising platforms for investigating proximity effects [54]. The weak interlayer coupling in vdW materials allows for layer-by-layer assembly of heterostructures

with tailored parameters. Numerous vdW materials are now available, including magnets (e.g., Fe_3GeTe_2 [55–63], VSe_2 [64, 65], CrTe_2 [66], V_5S_8 [67], VS_2 [65]) and superconductors (e.g., NbSe_2 [68, 69], MoS_2 [70]). Several theoretical [71–76] and experimental [77–81] studies have explored S/F vdW heterostructures. In particular, Refs. [73] and [74] have theoretically investigated the proximity effect in S/F structures with single or few superconducting monolayers, revealing counterintuitive non-monotonic dependence of superconductivity on the internal exchange field and gate voltage applied to the ferromagnet.

Several theoretical works have been dedicated to the SVE in heterostructures consisting of a few monolayers. Standard, inverse, and triplet SVE have been reported depending on the material and geometric parameters of the trilayer [82–86]. In this work, we demonstrate that vdW heterostructures provide a versatile platform for implementing all types of SVE—standard, inverse, and triplet—in the *same* structure. The type of SVE can be controlled by a gate potential applied to the F_1 and F_2 layers of the $F_1/\text{S}/F_2$ heterostructure, which adjusts the chemical potentials $\mu_{F_{1(2)}}$ of the respective ferromagnetic layers.

By considering a minimal model of the vdW trilayer, we study the full phase diagram of the system in the (μ_{F_1}, μ_{F_2}) -plane, revealing regions of standard, inverse, and triplet SVE. The physical mechanism underlying the controllability of the SVE is discussed. Moreover, we demonstrate that in the considered $F_1/\text{S}/F_2$ vdW heterostructure, the temperature dependence of the superconducting order parameter (OP) is also widely tunable by gating, even in the most easily realizable experimental case of parallel magnetizations. Depending on the gate voltages applied to the F_1 and F_2 layers, superconductivity can exhibit exotic behavior strongly different from standard BCS-like suppression. In particular, we obtain reentrant superconductivity, regions of bistable behavior, appearance of superconductivity at finite temperatures, and first-order superconducting transitions.

The paper is organized as follows. In Sec. II, we introduce the theoretical model for the heterostructure. Sec. III outlines the Green’s function formalism employed in our calculations. We present our findings on the gate-tunable standard and inverse SVE and discuss the underlying physical mechanism in Sec. IV. The triplet spin-valve effect is analyzed in Sec. V. Sec. VI explores the potential for realizing non-trivial, non-BCS temperature dependencies of the superconducting order parameter through gating. Finally, Sec. VII provides the conclusions of our work. Technical details concerning the derivation of the Gor’kov equation for the Green’s function are provided in Appendix A, while the numerical results for the temperature dependence of the order parameter are presented in Appendix B.

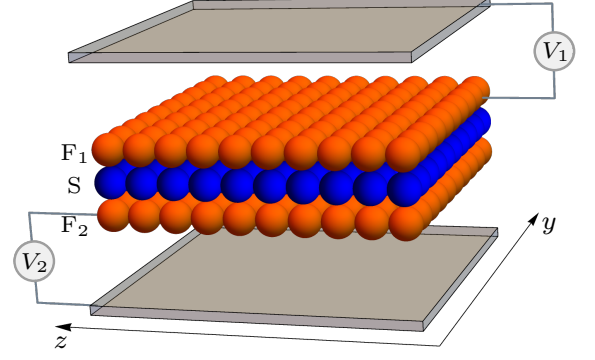


FIG. 1. **$F_1/\text{S}/F_2$ van der Waals spin valve.** The heterostructure comprises a monolayer superconductor (S) encapsulated between two ferromagnetic monolayers (F_1 and F_2). Schematic representation includes top and bottom gate voltages $V_{1,2}$ applied to the respective $F_{1,2}$ layers.

II. MODEL

The system under investigation is schematically depicted in Fig. 1. It comprises a monolayer superconducting sheet sandwiched between two monolayer ferromagnetic films, forming a prototypical $F_1/\text{S}/F_2$ superconducting spin valve. The system is modeled by a tight-binding Hamiltonian on a square lattice:

$$H = H_{F_1} + H_{F_2} + H_S + H_{FS}, \quad (1)$$

where the Hamiltonian for the ferromagnetic layer F_n ($n = 1, 2$) is given by

$$H_{F_n} = -t_F \sum_{\langle ij \rangle, \sigma} c_{i\sigma}^{F_n \dagger} c_{j\sigma}^{F_n} - \mu_{F_n} \sum_{i, \sigma} c_{i\sigma}^{F_n \dagger} c_{i\sigma}^{F_n} + \sum_{i, \alpha, \beta} c_{i\alpha}^{F_n \dagger} (\mathbf{h}_n \cdot \boldsymbol{\sigma})_{\alpha\beta} c_{i\beta}^{F_n}, \quad (2)$$

the superconducting layer Hamiltonian reads

$$H_S = -t_S \sum_{\langle ij \rangle, \sigma} c_{i\sigma}^S c_{j\sigma}^S - \mu_S \sum_{i, \sigma} c_{i\sigma}^S c_{i\sigma}^S + \sum_i (\Delta c_{i\uparrow}^S c_{i\downarrow}^S + \text{h.c.}), \quad (3)$$

and the interlayer coupling is described by

$$H_{FS} = -t_{FS} \sum_{i, \sigma, n} (c_{i\sigma}^{F_n \dagger} c_{i\sigma}^S + \text{h.c.}). \quad (4)$$

Here, $c_{i\sigma}^S$ ($c_{i\sigma}^{F_n}$) denotes the electron annihilation operator in the S (F_n) layer at site i with spin $\sigma = \uparrow, \downarrow$. The parameters μ_S and μ_{F_n} represent the onsite energies of the S and F_n layers, respectively, measured from the bottom of their corresponding conduction bands. For an isolated layer, the onsite energy coincides with its chemical potential. We consider only nearest-neighbor hopping, with

t_S (t_F) being the intralayer hopping integral within the S (F_n) material. The notation $\langle \mathbf{i}\mathbf{j} \rangle$ indicates summation over nearest-neighbor sites, and t_{FS} quantifies the interlayer hopping between S and F_n layers. The exchange field \mathbf{h}_n in layer F_n is taken as spatially uniform within the plane. The ferromagnetic layers are assumed identical with $h_1 = h_2 = h$, though our results can be readily extended to accommodate different magnetization magnitudes $h_1 \neq h_2$, as will be discussed in Sec. IV. The superconducting OP Δ , assumed to be of spin-singlet s -wave type and non-zero only in the S layer, is determined self-consistently via $\Delta = \lambda \langle c_{i\downarrow}^S c_{i\uparrow}^S \rangle$, where λ is the pairing constant.

The magnetization vectors \mathbf{h}_1 and \mathbf{h}_2 are confined to the yz -plane, with an angle θ between them. Their orientations in spin space are defined as:

$$\mathbf{h}_{1,2} = h(0, \pm \sin(\theta/2), \cos(\theta/2))^T. \quad (5)$$

It is important to note that the absence of spin-orbit coupling in our model renders the spin and coordinate spaces independent. Consequently, the plane spanned by the magnetization vectors \mathbf{h}_1 and \mathbf{h}_2 can be chosen arbitrarily with respect to the S/ F_n interfaces. We set $t_F/t_S = 1.25$ and $t_{FS} \ll t_{F,S}$. This parameter choice captures the essential qualitative characteristics of the electronic spectra in vdW materials near the Fermi level. Density functional theory (DFT) calculations [87], for instance, indicate that interlayer hopping in NbSe₂ is roughly an order of magnitude smaller than intralayer

hopping. Moreover, hopping between dissimilar materials is expected to be further reduced [73] due to lattice mismatch and interface imperfections.

The primary objective of this work is to explore the gate-tunability of the superconducting state in the spin valve. In mono- or few-layer vdW materials, gating provides an effective means to modulate the chemical potential [61, 88, 89]. Accordingly, within our model, the ferromagnetic onsite energies $\mu_{F1,2}$ are treated as external parameters, with their variations proportional to the applied top (V_1) and bottom (V_2) gate voltages, respectively.

While the model studied here is relatively simple and omits certain realistic features of vdW materials—such as Ising or Rashba spin-orbit coupling, which can be crucial for phenomena like finite-momentum pairing (Fulde-Ferrell-Larkin-Ovchinnikov state) [90–95] or dissipationless spin transport [75]—it adequately captures the essential physics of the magnetic proximity effect and its impact on the superconducting order parameter and correlations, as it has been previously demonstrated for F/S bilayer structures with monolayer components [73].

III. GREEN'S FUNCTIONS TECHNIQUE FOR F/S/F VDW HETEROSTRUCTURE

We introduce the Nambu spinor

$$\check{\psi}_{\mathbf{i}} = (c_{i\uparrow}^{F_1}, c_{i\downarrow}^{F_1}, c_{i\downarrow}^{F_1\dagger}, -c_{i\uparrow}^{F_1\dagger}, c_{i\uparrow}^S, c_{i\downarrow}^S, c_{i\downarrow}^{S\dagger}, -c_{i\uparrow}^{S\dagger}, c_{i\uparrow}^{F_2}, c_{i\downarrow}^{F_2}, c_{i\downarrow}^{F_2\dagger}, -c_{i\uparrow}^{F_2\dagger})^T \quad (6)$$

and define the Green's function—a 12×12 matrix in the direct product of spin, particle-hole, and layer spaces—as follows:

$$\check{G}_{\mathbf{i}\mathbf{j}}(\tau_1, \tau_2) = -\tau_z \langle T_\tau \check{\psi}_{\mathbf{i}}(\tau_1) \check{\psi}_{\mathbf{j}}^\dagger(\tau_2) \rangle, \quad (7)$$

where $\langle T_\tau \dots \rangle$ denotes imaginary time-ordered thermal averaging. Throughout this work, we employ Pauli matrices σ_k and τ_k ($k = 0, x, y, z$) in spin and particle-hole spaces, respectively.

Owing to the translational invariance along the S/F

interface, we introduce the Fourier-transformed Green's function:

$$\check{G}(\mathbf{p}, \tau) = \int d^2r e^{-i\mathbf{p}(\mathbf{i}-\mathbf{j})} \check{G}_{\mathbf{i}\mathbf{j}}, \quad (8)$$

with $\tau = \tau_1 - \tau_2$ and integration performed over $\mathbf{i} - \mathbf{j}$.

Expanding $\check{G}(\mathbf{p}, \tau)$ in fermionic Matsubara frequencies $\omega_m = \pi T(2m+1)$ as $\check{G}(\mathbf{p}, \tau) = T \sum_{\omega_m} e^{-i\omega_m \tau} \check{G}(\mathbf{p}, \omega_m)$, where T is the temperature, we derive the Gor'kov equation for the Green's function [see Appendix A for details]:

$$\check{G}^{-1} \check{G}(\mathbf{p}, \omega_m) = 1, \quad (9)$$

$$\check{G}^{-1} = \begin{pmatrix} i\omega_m \tau_z - \xi_{F_1} - \mathbf{h}_1 \boldsymbol{\sigma} \tau_z & t_{FS} & 0 \\ t_{FS} & i\omega_m \tau_z - \xi_S + i\Delta \tau_y & t_{FS} \\ 0 & t_{FS} & i\omega_m \tau_z - \xi_{F_2} - \mathbf{h}_2 \boldsymbol{\sigma} \tau_z \end{pmatrix}, \quad (10)$$

where

$$\xi_S = -2t_S(\cos p_y a + \cos p_z a) - \mu_S \quad (11)$$

and

$$\xi_{F_{1(2)}} = -2t_F(\cos p_y a + \cos p_z a) - \mu_{F_{1(2)}} \quad (12)$$

represent the normal-state electron spectra of the S and $F_{1(2)}$ layers, respectively, and a is the lattice constant. Each element of the matrix in Eq. (10) is a 4×4 matrix in the direct product of particle-hole and spin spaces, with the explicit layer-space structure shown.

The superconducting order parameter, taken to be real, is determined from the self-consistency equation

$$\Delta = \lambda T \sum_{\omega_m} \int \frac{d^2 p}{(2\pi)^2} \frac{\text{Tr}[\check{G}^{SS}(\mathbf{p}, \omega_m) \sigma_0 \tau_-]}{2}, \quad (13)$$

where λ is the dimensionless BCS coupling constant, $\tau_- = (\tau_x - i\tau_y)/2$, and \check{G}^{SS} denotes the $(2, 2)$ -element of $\check{G}(\mathbf{p}, \omega_m)$ in layer space—a 4×4 matrix in particle-hole and spin spaces representing the Green's function of the superconducting layer.

The electronic spectral density in the S-layer for the parallel magnetization configuration ($\theta = 0$) and spin $\sigma = \pm 1$ is given by

$$A_\sigma(\varepsilon, \mathbf{p}) = -\frac{1}{\pi} \text{Im} \left[\frac{\text{Tr}[\check{G}^{R,SS}(\sigma_0 + \sigma\sigma_z)(\tau_0 + \tau_z)]}{4} \right], \quad (14)$$

where $\check{G}^{R,SS}$ is obtained from \check{G}^{SS} via analytic continuation $i\omega_m \rightarrow \varepsilon + i\delta$, with δ a positive infinitesimal.

For the antiparallel magnetization configuration ($\theta = \pi$), where the magnetization vectors align along the y -axis, the spectral density becomes

$$A_\sigma(\varepsilon, \mathbf{p}) = -\frac{1}{\pi} \text{Im} \left[\frac{\text{Tr}[\check{G}^{R,SS}(\sigma_0 + \sigma\sigma_y)(\tau_0 + \tau_z)]}{4} \right]. \quad (15)$$

We further examine the singlet and triplet correlations in the S layer, computed as

$$d_k(\omega_m) = \int \frac{d^2 p}{(2\pi)^2} \frac{\text{Tr}[\check{G}^{SS}(\mathbf{p}, \omega_m) \sigma_k \tau_-]}{2}, \quad (16)$$

where d_0 represents the singlet correlation amplitude, and the vector $\mathbf{d} = (d_x, d_y, d_z)^T$ characterizes the triplet superconducting correlations. In the present system, d_x becomes nonzero only for non-collinear magnetizations \mathbf{h}_1 and \mathbf{h}_2 , signaling the non-collinear (triplet) spin-valve effect. The components d_y and d_z , in contrast, are associated with the standard and inverse spin-valve effects, respectively.

IV. GATE-CONTROLLED STANDARD AND INVERSE SPIN-VALVE EFFECTS

One of central findings of our work is the demonstration that switching between standard and inverse SVE can be achieved by electrically gating either ferromagnetic layer to modulate its on-site energy. Fig. 2 presents a phase diagram mapping the regions in (μ_{F_1}, μ_{F_2}) parameter space where standard and inverse SVE are realized within our model framework. Fig. 3(a) displays

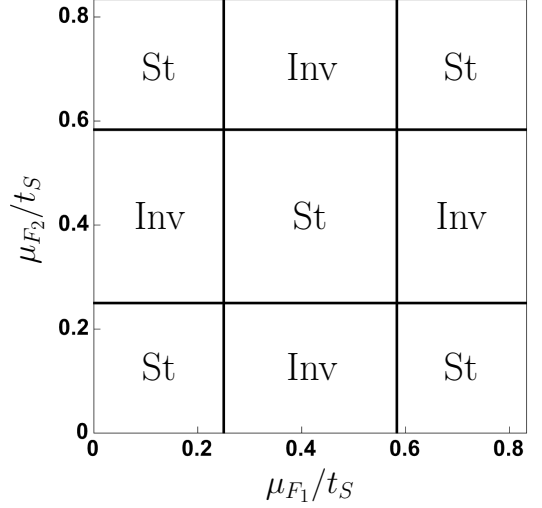


FIG. 2. **Phase diagram for standard and inverse SVE.** The diagram delineates the regions in the (μ_{F_1}, μ_{F_2}) parameter space where the standard (St) and inverse (Inv) SVEs are realized. Parameters used: $t_F = 1.25t_S$, $t_{FS} = 0.017t_S$, $\mu_S = 0.333t_S$, and $h = 0.167t_S$.

a characteristic dependence of T_c on the on-site energy of one of the ferromagnetic layers for both parallel (T_c^P , blue) and antiparallel (T_c^{AP} , orange) magnetization configurations. The distinct behavior of the blue and orange curves reveals that the system exhibits standard SVE ($T_c^{AP} > T_c^P$) or inverse SVE ($T_c^{AP} < T_c^P$) depending on the value of μ_{F_2} . Notably, near the boundaries separating standard and inverse SVE regions—where superconductivity suppression is most pronounced—we observe absolute SVE, characterized by either $T_c^{AP} = 0$ with $T_c^P \neq 0$ or vice versa. Assuming $\Delta_0 \sim 10$ K ~ 1 meV, the full studied range corresponds to $\Delta\mu_{F_{1,2}} \sim 50$ meV, with absolute SVE regions spanning $\delta\mu_{F_{1,2}} \sim 1$ meV. This indicates that different SVE types, including absolute SVE, can be continuously tuned via gating.

The inset to Fig. 3(a) shows an expanded view of a region of suppressed superconductivity for the parallel configuration. It reveals a non-trivial, cusp-like suppression of T_c , which signals a departure from conventional BCS-like behavior and indicates the presence of bistable and reentrant superconducting states as a function of temperature, as discussed in detail in Sec. VI.

The gate-tunability of the SVE is fundamentally rooted in the electronic band hybridization that governs proximity effects in few-layer van der Waals heterostructures [73]. To elucidate the underlying mechanism, Figs. 3(b)-(e) present the spin-resolved electronic spectral density calculated for system parameters corresponding to points b-e in Fig. 3(a). The spectral densities for parallel and antiparallel magnetization configurations were calculated using Eqs. (14) and (15), respectively. Within our simplified model framework, it is advantageous to represent the spectra as a function of

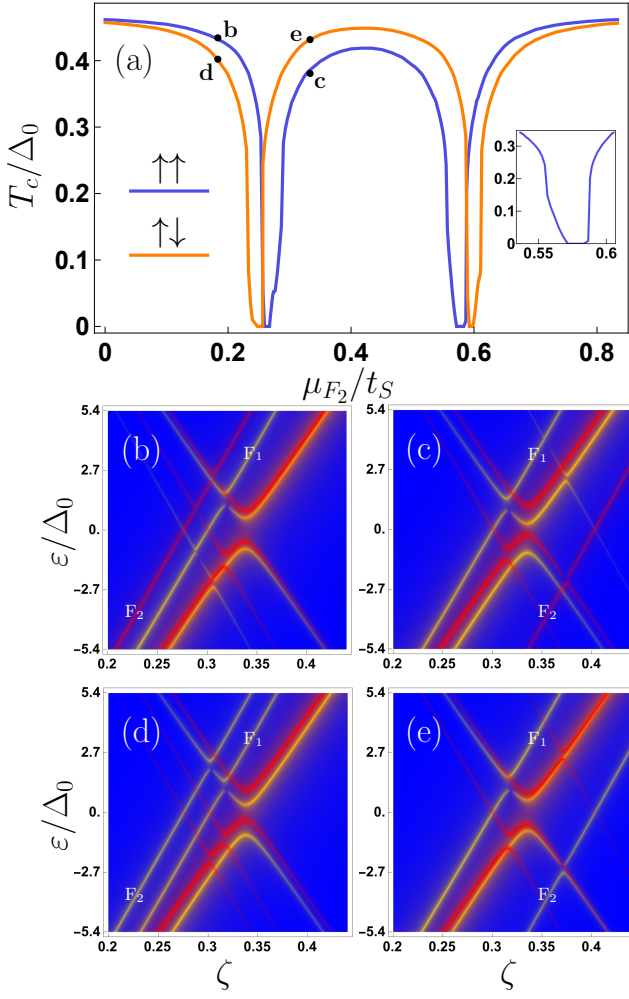


FIG. 3. T_c and electronic spectra of the $F_1/S/F_2$ spin valve. (a) Superconducting critical temperature T_c versus the on-site energy μ_{F_2} of the bottom ferromagnetic layer for parallel (blue) and antiparallel (orange) magnetization configurations. Inset: expanded view of the right region of suppressed superconductivity for the parallel configuration. (b)–(e) Spin-resolved electronic spectral density for spin-up (yellow) and spin-down (red) states as a function of quasi-particle energy ε and $\zeta = -2(\cos p_y a + \cos p_z a)$, calculated at the μ_{F_2} values marked by points b–e in panel (a). Spectral branches associated with the F_1 and F_2 layers are labeled accordingly. Here, Δ_0 denotes the superconducting order parameter at $T = 0$. Parameters: $T = 0.214\Delta_0$, $\Delta_0 = 0.016t_S$, $t_F = 1.25t_S$, $t_{FS} = 0.017t_S$, $\mu_S = 0.333t_S$, $\mu_{F_1} = 0.55t_S$, $h = 0.167t_S$. Specific values: (b),(d) $\mu_{F_2} = 0.183t_S$; (c),(e) $\mu_{F_2} = 0.333t_S$.

$\zeta = -2(\cos p_y a + \cos p_z a)$ rather than along specific momentum directions. Hyperbolic spectral branches originate from the superconductor, while each ferromagnet contributes two spin-split linear branches, one of which is visible and labeled accordingly; the remaining ferromagnetic branches lie outside the displayed (ζ, ε) range.

Finite interlayer hopping t_{FS} causes hybridization

between superconducting and ferromagnetic branches, yielding a Zeeman splitting of the superconducting branches that is determined by the relative alignment of the superconducting and ferromagnetic spectral branches. Neglecting t_{FS} , the ferromagnetic branch follows $\xi_{F_{1,2}}^\sigma = t_F \zeta - \mu_{F_{1,2}} + \sigma h$ [see Eqs. (10) and (12)], implying that the relative alignment between ferromagnetic ($F_{1,2}$) and superconducting branches is governed by the on-site energy $\mu_{F_{1,2}}$.

The spin splitting of superconducting branches can be quantified by the effective exchange field h_{eff} induced in the S-layer by the ferromagnets. Qualitatively, h_{eff} can be approximated as a superposition of contributions from individual ferromagnetic layers, though rigorous calculations account for their mutual influence—generally weak across broad parameter ranges and negligible for qualitative analysis. In the limit of weak interlayer hopping $t_{FS} \ll |\xi_F^\sigma(\zeta_0)|$, with ζ_0 determined by $\xi_S(\zeta_0) = 0$, the effective exchange field induced by a ferromagnet in an S/F heterostructure takes the form [74]:

$$h_{eff} = \frac{-ht_{FS}^2}{\xi_F^+(\zeta_0)\xi_F^-(\zeta_0)} = \frac{ht_{FS}^2}{h^2 - [(\mu_S t_F/t_S) - \mu_F]^2}. \quad (17)$$

Maximal spin splitting of superconducting branches occurs when $\xi_F^\sigma(\zeta_0) = 0$, i.e., when a superconducting branch crosses a ferromagnetic branch at the Fermi level $\varepsilon = 0$ (though Eq. (17) becomes inaccurate in this regime). Furthermore, the splitting changes sign as ξ_F^σ changes sign, which occurs when a ferromagnetic branch passes through the superconducting branch upon variation of the corresponding on-site energy. This sign reversal underlies the SVE switching observed between points b–d and e–c in Fig. 3(a). At point b, the h_{eff} contributions from F_1 and F_2 partially cancel [Fig. 3(b)], whereas at point c they add constructively despite *unchanged parallel magnetization alignment*. An analogous but reversed sequence applies to the antiparallel configuration [Figs. 3(d)–(e)].

These findings remain robust against variations in model parameters, including non-identical ferromagnets. Altering parameters such as h_1 , h_2 , or μ_S merely shifts the μ_{F_1} and μ_{F_2} values at which strongest hybridization occurs, consequently displacing the regions of maximal T_c suppression in Fig. 3(a) and shifting the boundaries between standard and inverse SVE regions in Fig. 2.

V. GATE-CONTROLLED TRIPLET SPIN-VALVE EFFECT

The triplet SVE—also referred to as the non-monotonic SVE—manifests as a non-monotonic dependence of both the order parameter Δ and the critical temperature T_c on the magnetization misorientation angle θ . As noted in the introduction, the characteristic minimum in $T_c(\theta)$ or $\Delta(\theta)$ arises from the generation of spin-triplet correlations with a \mathbf{d} -vector proportional

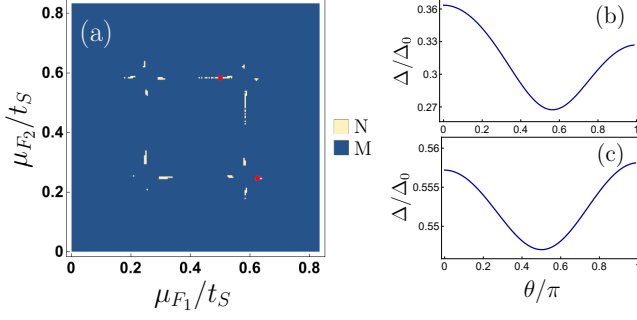


FIG. 4. **Non-monotonic angular dependence of the superconducting order parameter.** (a) Phase diagram indicating regions of monotonic (M) and non-monotonic (N) $\Delta(\theta)$ behavior. (b,c) Examples of non-monotonic $\Delta(\theta)$ dependencies corresponding to the red points in panel (a): (b) $\mu_{F1} = 0.625t_S$, $\mu_{F2} = 0.247t_S$; (c) $\mu_{F1} = 0.5t_S$, $\mu_{F2} = 0.583t_S$. Other parameters are the same as in Fig. (3).

to $\mathbf{h}_1 \times \mathbf{h}_2$. These correlations correspond to equal-spin triplet pairs when quantized along an axis parallel to the total effective exchange field in the superconductor, i.e., along $\mathbf{h}_1 + \mathbf{h}_2$ or $\mathbf{h}_1 - \mathbf{h}_2$. In conventional multilayer ferromagnets, such triplets are often termed long-range triplet correlations [2], as their amplitude decays much more slowly into the ferromagnet than that of opposite-spin pairs with $\mathbf{d} \parallel \mathbf{h}$. However, in the present monolayer system, the distinction between short- and long-range triplet components is no longer meaningful. The emergence of $\mathbf{h}_1 \times \mathbf{h}_2$ pairs opens an additional singlet-triplet conversion channel, further suppressing singlet superconductivity. These triplet correlations peak near $\theta = \pi/2$ resulting in the strongest suppression of superconductivity.

Figure 4(a) identifies the regions in the (μ_{F1}, μ_{F2}) -plane where the triplet SVE is realized within our model. Representative examples of non-monotonic $\Delta(\theta)$ are shown in Figs. 4(b)–(c). Although the regions supporting the triplet SVE appear relatively narrow, their accessibility via continuous gate-voltage tuning of the on-site energies facilitates experimental observation.

To gain further insight into the proximity effect in the vdW spin valve, we plot the phase diagrams of singlet (d_0) and triplet (\mathbf{d}) superconducting correlations in Figs. 5(a)–(d). These results, calculated self-consistently via Eq. (16) at $\theta = \pi/2$, show that singlet correlations suppression is most pronounced in regions where the electronic spectra of the S and one of the F layers hybridize strongly, i.e., where $\xi_F^\sigma(\zeta_0) = 0$. When this condition is met for both ferromagnetic layers simultaneously, singlet correlations and the order parameter are completely suppressed [blue regions in Fig. 5(a)].

The triplet component proportional to $\mathbf{h}_1 \times \mathbf{h}_2$, which in our geometry aligns with the x -axis, is presented in Fig. 5(b). This component reaches its maximum amplitude in regions of strong hybridization, consistent with

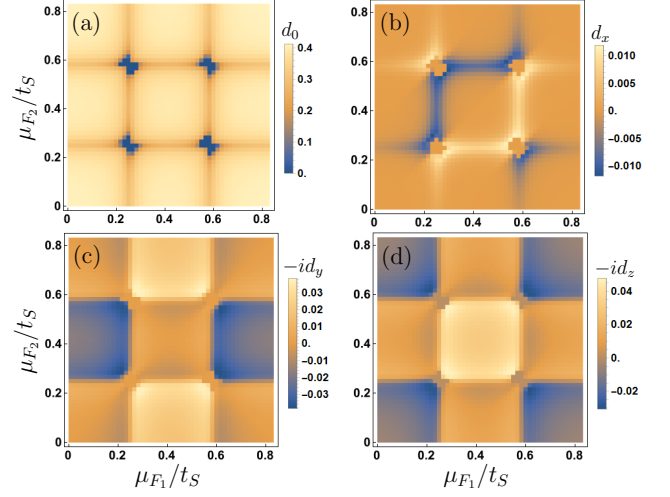


FIG. 5. **Singlet and triplet superconducting correlations as functions of (μ_{F1}, μ_{F2}) .** (a) Singlet correlations $d_0(\omega_0)$ at the first Matsubara frequency, (b) triplet correlations $d_x(\omega_0)$, (c) triplet correlations $-id_y(\omega_0)$, (d) triplet correlations $-id_z(\omega_0)$. $\theta = \pi/2$. Other parameters are the same as in Fig. (3).

the suppression of singlet correlations. The d_x correlations exhibit antisymmetry under the exchange $\mu_{F1} \leftrightarrow \mu_{F2}$, as required by symmetry considerations. Specifically, a π -rotation of the spin valve about the z -axis exchanges μ_{F1} and μ_{F2} and reverses the sign of d_x , leaving the exchange fields unchanged. The magnitude of d_x is several times smaller than that of the other correlation components. In the limit of weak interlayer hopping $t_{FS} \ll (t_{S,F}, \mu_{S,F1,2}, \Delta, T)$, the analytical expression for d_x takes the form:

$$d_x \approx \frac{4 t_{FS}^4 \omega_m \Delta (\mathbf{h}_1 \times \mathbf{h}_2)_x (\mu_{F2} - \mu_{F1})}{(\Delta^2 + \mu_S^2 + \omega_m^2)^2} \times \prod_{\gamma=\pm 1} \frac{\sqrt{h^2 + \mu_{F1} \mu_{F2} + \omega_m^2}}{[h^2 - (\mu_{F1} + \gamma i \omega_m)^2][h^2 - (\mu_{F2} + \gamma i \omega_m)^2]}. \quad (18)$$

Figs. 5(c) and (d) display the triplet correlations d_y and d_z , respectively. Away from the immediate vicinity of the strong hybridization regions ($\xi_F^\sigma(\zeta_0) = 0$), only one of the two components— d_y or d_z —is non-zero. This behavior stems from the alignment of these triplet components with the total effective field $\mathbf{h}_s = \mathbf{h}_{eff,1} + \mathbf{h}_{eff,2}$ induced in the S layer. When the effective fields $\mathbf{h}_{eff,1(2)}$ induced by each of the $F_{1,2}$ separately are both parallel or both antiparallel to $\mathbf{h}_{1(2)}$, the total field \mathbf{h}_s lies along the z -axis. Conversely, if $\mathbf{h}_{eff,1}$ is antiparallel to \mathbf{h}_1 while $\mathbf{h}_{eff,2}$ is parallel to \mathbf{h}_2 (or vice versa), \mathbf{h}_s aligns with the y -axis.

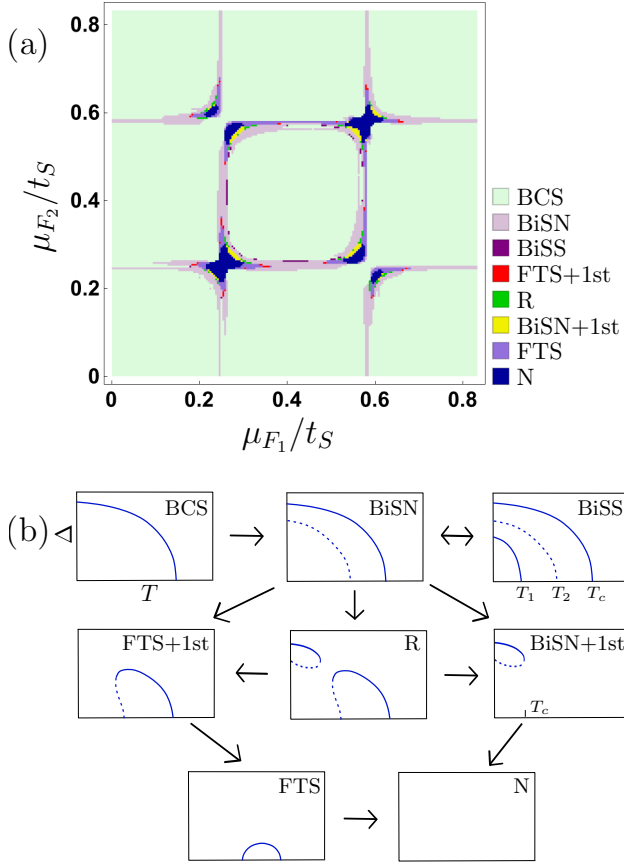


FIG. 6. (a) Phase diagram in the (μ_{F1}, μ_{F2}) plane identifying regions hosting distinct temperature-dependent behaviors of the order parameter. Parallel magnetic configuration. Color-coded areas correspond to the different regimes identified, see the legend. (d) Schematic illustration of the possible evolution of $\Delta(T)$, attainable by gating, from an unsuppressed BCS-like superconducting state to the fully suppressed normal state. Each curve qualitatively represents the characteristic temperature dependence within the corresponding phase identified in panel (a). All parameters except for $\mu_{F1,2}$ are the same as in Fig. (3).

VI. TEMPERATURE DEPENDENCE OF THE SUPERCONDUCTING ORDER PARAMETER

As noted in the introduction, the temperature dependence of the order parameter is highly tunable by gating, even for the parallel magnetization configuration ($\theta = 0$). Fig. 6(a) presents the complete phase diagram in the (μ_{F1}, μ_{F2}) -plane, identifying regions where different types of temperature-dependent OP behavior emerge within our model. Depending on the values of (μ_{F1}, μ_{F2}) , we distinguish: conventional BCS-like suppression (BCS); bistable states with two stable superconducting solutions (BiSS) or coexisting superconducting and normal states (BiSN); first-order transitions between superconducting and normal states (1st); reentrant

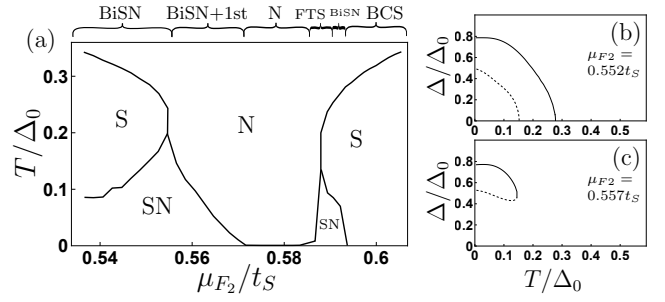


FIG. 7. (a) Phase diagram in the (μ_{F2}, T) plane for the region of suppressed superconductivity, corresponding to the area magnified in the inset of Fig. 3(a). The top of the panel indicates the specific phases realized within each interval of μ_{F2} . Lines separate regions where only the superconducting state (S), both superconducting and normal states (SN), or only the normal state (N) are stable. (b)–(c) Representative examples of the temperature evolution of the order parameter $\Delta(T)$, as discussed in the main text.

superconductivity (R); and the emergence of superconductivity at finite temperature (FTS).

Figure 6(b) illustrates all possible types of $\Delta(T)$ evolution accessible by varying the ferromagnetic on-site energies. Beginning from the conventional BCS regime and adjusting (μ_{F1}, μ_{F2}) via gating, superconductivity can be fully suppressed through various intermediate non-BCS states, as listed above. Schematic curves depict characteristic $\Delta(T)$ behaviors in each region; numerically calculated examples at specific (μ_{F1}, μ_{F2}) points are provided in Appendix B.

The listed above phases are classified according to the most important characteristic features. For example, for the BiSS-phase the system has two stable superconducting solutions only at $T < T_1$, and at $T_1 < T < T_2$ [see picture BiSS in Fig. 6(b)] two stable solutions of the system are superconducting and normal. In this sense at $T_1 < T < T_2$ the BiSS-phase is identical to the BiSN-phase. Some regions of the (μ_{F1}, μ_{F2}) -plane exhibit a combination of two phases according to our classification. For example, in the picture BiSN+1st we can see the BiSN phase at $T < T_c$, but the transition from the superconducting state to the normal state at $T = T_c$ is the first-order transition in contrast to the picture BiSN, where the transition is of the second order. In separate points of the (μ_{F1}, μ_{F2}) -plane we also found more subtle features of $\Delta(T)$ behavior. For example, the BCS-like behavior can start from a small region of growing $\Delta(T)$ at low temperatures, see Appendix B.

Given the identification of the possible superconducting phases realizable via gating in our spin-valve system, we can now interpret the nontrivial, cusp-like suppression of T_c presented in the inset of Fig. 3(a). The phase diagram in the (μ_{F2}, T) -plane for the region of suppressed superconductivity is shown in Fig. 7(a). At small μ_{F2} , the system resides in a bistable superconducting/normal

(BiSN) state. This implies that at low temperatures, both superconducting and normal states are thermodynamically stable [SN region in Fig. 7(a)], while at higher temperatures only the superconducting phase is stable [S region in Fig. 7(a)]. An example of $\Delta(T)$ curve for this regime is displayed in Fig. 7(b). Owing to the non-BCS temperature dependence of the order parameter, the superconducting-to-normal transition does not occur directly but proceeds through an intermediate phase combining bistability and a first-order transition (BiSN+1st), as seen in Fig. 7(b). The cusp in the $T_c(\mu_{F_2})$ dependence highlighted in the inset of Fig. 3(a) is a direct consequence of this transition between different superconducting phases.

Various forms of non-BCS superconductivity have been previously proposed. Notable examples include bistable BiSN states and first-order phase transitions in thin-film S/F heterostructures [96], thin superconducting films under parallel magnetic fields [97], reentrant superconductivity in S/F bilayers [98–100], and the emergence of superconductivity at finite temperatures under non-equilibrium conditions [101]. The fundamental significance and experimental advantage of our F/S/F trilayer lie in its capacity to host all these exotic superconducting states within a single, fully controllable system. Crucially, these states can be accessed through smooth adjustment of external gate voltages, without imposing stringent constraints on the system parameters.

VII. CONCLUSIONS

In summary, we have demonstrated that van der Waals $F_1/S/F_2$ trilayers provide a highly versatile platform for implementing and controlling various types of superconducting spin-valve effects through electrostatic gating. Our theoretical investigation, based on a minimal tight-binding model and Green's function approach, reveals several key findings:

First, the standard, inverse, and triplet spin-valve effects can all be realized within the same heterostructure by tuning the onsite energies of the ferromagnetic layers via gate voltages. The transitions between these regimes are governed by the hybridization between superconducting and ferromagnetic electronic spectra, which determines the effective exchange field induced in the superconducting layer.

Second, the gate control extends beyond the spin-valve functionality to the fundamental temperature dependence of the superconducting order parameter. Even

for parallel magnetization alignment, we observe a rich variety of non-BCS behaviors including reentrant superconductivity, bistable states, first-order phase transitions, and the emergence of superconductivity at finite temperatures.

The accessibility of different spin-valve regimes and the exotic superconducting states through smooth gate voltage adjustments, without requiring stringent parameter constraints, highlights the unique advantages of van der Waals heterostructures for superconducting spintronics. The predicted effects are experimentally relevant, given the established capabilities for electrostatic gating in few-layer materials and the recent progress in fabricating high-quality van der Waals heterostructures.

Our work establishes gate-tunable van der Waals spin valves as promising building blocks for future superconducting spintronic devices, offering unprecedented electrical control over superconducting phenomena and opening new avenues for exploring the rich physics of proximity effects in low-dimensional systems.

ACKNOWLEDGMENTS

A.S.I., G.A.B. and I.V.B. acknowledge the support from Theoretical Physics and Mathematics Advancement Foundation “BASIS” via the project No. 23-1-1-51-1. The calculations of the gate-controllable spin valve effect were supported by the Russian Science Foundation via the project No. 24-12-00152. The study of the gate-controlled temperature dependence of the order parameter has been performed under the support by Grant from the ministry of science and higher education of the Russian Federation No. 075-15-2025-010.

Appendix A: Derivation of the Gor'kov equation for a F/S/F vdW heterostructure

In this section we present key steps of the derivation of the Gor'kov equation for the trilayer heterostructure. The Green's function Eq. (7) obeys the following equation:

$$\frac{d\check{G}_{ij}}{d\tau_1} = -\delta(\tau_1 - \tau_2)\delta_{ij} - \tau_z \langle T_\tau \frac{d\check{\psi}_i(\tau_1)}{d\tau_1} \check{\psi}_j^\dagger(\tau_2) \rangle. \quad (A1)$$

For the system described by Hamiltonian (1) the Heisenberg equation of motion for spinor $\check{\psi}_i$ takes the form:

$$\frac{d\check{\psi}_i}{d\tau} = [\hat{H}, \check{\psi}_i] = \hat{M}\check{\psi}_i = \begin{pmatrix} t_F\hat{t}\tau_z + \mu_{F_1}\tau_z - \mathbf{h}_1\boldsymbol{\sigma} & t_{FS}\tau_z & 0 \\ t_{FS}\tau_z & t_S\hat{t}\tau_z + \mu_{S}\tau_z - \tilde{\Delta} & t_{FS}\tau_z \\ 0 & t_{FS}\tau_z & t_F\hat{t}\tau_z + \mu_{F_2}\tau_z - \mathbf{h}_2\boldsymbol{\sigma} \end{pmatrix} \check{\psi}_i \quad (A2)$$

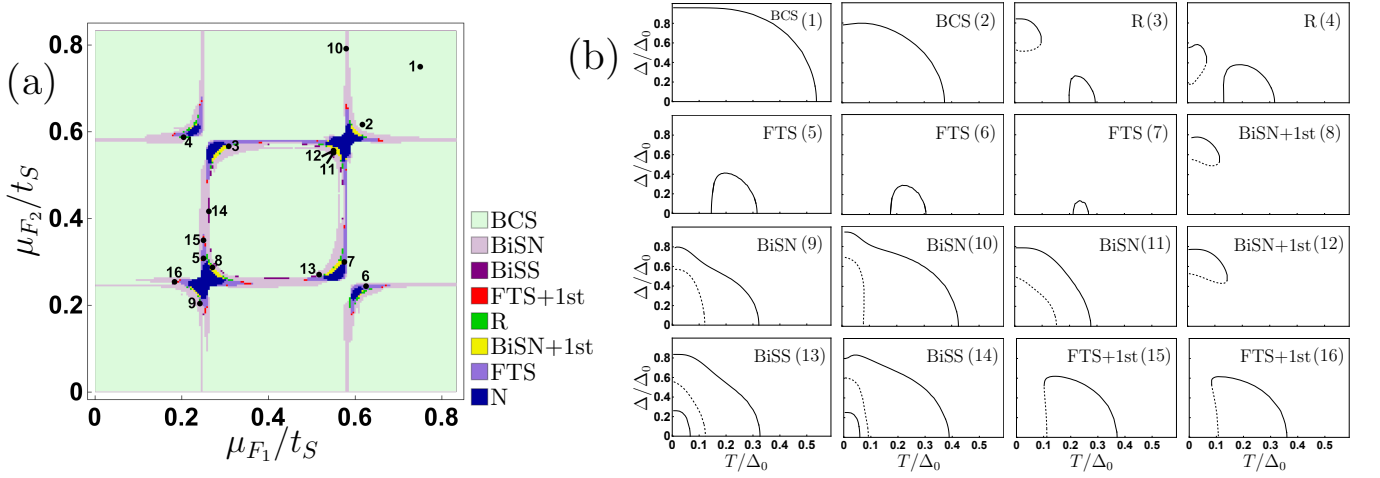


FIG. 8. (a) Phase diagram in the (μ_{F1}, μ_{F2}) plane identifying regions hosting distinct temperature-dependent behaviors of the order parameter. (b) Specific examples of $\Delta(T)$ behavior corresponding to (μ_{F1}, μ_{F2}) -points marked in panel (a) by numbers (1) $\mu_{F1} = 0.75t_S, \mu_{F2} = 0.75t_S$, (2) $\mu_{F1} = 0.617t_S, \mu_{F2} = 0.617t_S$, (3) $\mu_{F1} = 0.308t_S, \mu_{F2} = 0.567t_S$, (4) $\mu_{F1} = 0.204t_S, \mu_{F2} = 0.588t_S$, (5) $\mu_{F1} = 0.25t_S, \mu_{F2} = 0.308t_S$, (6) $\mu_{F1} = 0.625t_S, \mu_{F2} = 0.244t_S$, (7) $\mu_{F1} = 0.575t_S, \mu_{F2} = 0.3t_S$, (8) $\mu_{F1} = 0.271t_S, \mu_{F2} = 0.288t_S$, (9) $\mu_{F1} = 0.242t_S, \mu_{F2} = 0.204t_S$, (10) $\mu_{F1} = 0.579t_S, \mu_{F2} = 0.792t_S$, (11) $\mu_{F1} = 0.55t_S, \mu_{F2} = 0.552t_S$, (12) $\mu_{F1} = 0.55t_S, \mu_{F2} = 0.557t_S$, (13) $\mu_{F1} = 0.517t_S, \mu_{F2} = 0.271t_S$, (14) $\mu_{F1} = 0.263t_S, \mu_{F2} = 0.417t_S$, (15) $\mu_{F1} = 0.25t_S, \mu_{F2} = 0.35t_S$, (16) $\mu_{F1} = 0.183t_S, \mu_{F2} = 0.254t_S$. Other parameters are the same as in Fig. (3).

where $\tilde{\Delta} = \Delta\tau_+ + \Delta^*\tau_-$ with $\tau_{\pm} = (\tau_x \pm i\tau_y)/2$. The operator \hat{t} acts on the spinor $\tilde{\psi}_i$ in the following way:

$$\hat{t}\tilde{\psi}_i = \sum_{\langle ij \rangle} \tilde{\psi}_j = \sum_{\langle a \rangle} \tilde{\psi}_{i+a}. \quad (\text{A3})$$

Here $\mathbf{a} \in \{0, \pm\mathbf{a}_y, \pm\mathbf{a}_z\}$ are the basis vectors in the plane of the layers. Substituting Eq. (A2) into Eq. (A1) we obtain:

$$G_i^{-1} \tilde{G}_{ij}(\tau_1 - \tau_2) = \delta_{ij} \delta(\tau_1 - \tau_2), \quad (\text{A4})$$

$$G_i^{-1} = (\hat{M} - \frac{d}{d\tau_1})\tau_z. \quad (\text{A5})$$

The operator \hat{t} acts on the Green's function \tilde{G}_{ij} in the following way:

$$\hat{t}\tilde{G}_{ij} = \sum_a \tilde{G}_{i+a,j} \quad (\text{A6})$$

Further we introduce the Fourier transform of the Green's function as defined by Eq. (8). The term $\hat{j}\tilde{G}_{ij}$ in the momentum representation takes the form:

$$\sum_a \int d^2\mathbf{r} e^{-i\mathbf{p}(\mathbf{i}-\mathbf{j})} \tilde{G}_{i+a,j} = 2\tilde{G}(\mathbf{p}, \tau) [\cos(a_y p_y) + \cos(a_z p_z)], \quad (\text{A7})$$

where $\tau = \tau_1 - \tau_2$. Then, expanding the Green's function $\tilde{G}(\mathbf{p}, \tau)$ over fermionic Matsubara frequencies, one can obtain the Gor'kov equation for Green's function:

$$G_{\mathbf{p}}^{-1}(\omega_m) \tilde{G}(\mathbf{p}, \omega_m) = 1, \quad (\text{A8})$$

$$G_{\mathbf{p}}^{-1}(\omega_m) = (\hat{M}_{\mathbf{p}} + i\omega_m)\tau_z, \quad (\text{A9})$$

$$\hat{M}_{\mathbf{p}} = \begin{pmatrix} M_{\mathbf{p}}^{F_1} & t_{FS} & 0 \\ t_{FS} & M_{\mathbf{p}}^S & t_{FS} \\ 0 & t_{FS} & M_{\mathbf{p}}^{F_2} \end{pmatrix} \tau_z, \quad (\text{A10})$$

$$M_{\mathbf{p}}^{F_{1(2)}} = 2t_F [\cos(a_y p_y) + \cos(a_z p_z)] + \mu_{F_{1(2)}} - \mathbf{h}_{1(2)} \boldsymbol{\sigma} \tau_z, \quad (\text{A11})$$

$$M_{\mathbf{p}}^S = 2t_S [\cos(a_y p_y) + \cos(a_z p_z)] + \mu_S - \tilde{\Delta} \tau_z. \quad (\text{A12})$$

Appendix B: Temperature dependence of the superconducting OP: numerical results

In Fig. 8 we present numerically calculated examples of $\Delta(T)$ at some specific (μ_{F1}, μ_{F2}) points.

[1] A. I. Buzdin, Proximity effects in superconductor-ferromagnet heterostructures, Reviews of Modern

- [2] F. S. Bergeret, A. F. Volkov, and K. B. Efetov, Odd triplet superconductivity and related phenomena in superconductor-ferromagnet structures, *Rev. Mod. Phys.* **77**, 1321 (2005).
- [3] M. Eschrig, Spin-polarized supercurrents for spintronics: a review of current progress, *Reports on Progress in Physics* **78**, 104501 (2015).
- [4] J. Linder and J. W. A. Robinson, Superconducting spintronics, *Nature Physics* **11**, 307 (2015).
- [5] F. S. Bergeret, A. F. Volkov, and K. B. Efetov, Enhancement of the josephson current by an exchange field in superconductor-ferromagnet structures, *Phys. Rev. Lett.* **86**, 3140 (2001).
- [6] F. S. Bergeret, M. Silaev, P. Virtanen, and T. T. Heikkilä, Colloquium: Nonequilibrium effects in superconductors with a spin-splitting field, *Rev. Mod. Phys.* **90**, 041001 (2018).
- [7] P. De Gennes, Coupling between ferromagnets through a superconducting layer, *Physics Letters* **23**, 10 (1966).
- [8] L. R. Tagirov, Low-field superconducting spin switch based on a superconductor /ferromagnet multilayer, *Phys. Rev. Lett.* **83**, 2058 (1999).
- [9] A. I. Buzdin, A. V. Vedyayev, and N. V. Ryzhanova, Spin-orientation-dependent superconductivity in F/S/F structures, *Europhysics Letters* **48**, 686 (1999).
- [10] I. Baladié, A. Buzdin, N. Ryzhanova, and A. Vedyayev, Interplay of superconductivity and magnetism in superconductor/ferromagnet structures, *Phys. Rev. B* **63**, 054518 (2001).
- [11] I. Baladié and A. Buzdin, Thermodynamic properties of ferromagnet/superconductor/ferromagnet nanostructures, *Phys. Rev. B* **67**, 014523 (2003).
- [12] Y. V. Fominov, A. A. Golubov, and M. Y. Kupriyanov, Triplet proximity effect in FSF trilayers, *Journal of Experimental and Theoretical Physics Letters* 10.1134/1.1591981 (2003).
- [13] P. Cadden-Zimansky, Y. B. Bazaliy, L. M. Litvak, J. S. Jiang, J. Pearson, J. Y. Gu, C.-Y. You, M. R. Beasley, and S. D. Bader, Asymmetric ferromagnet-superconductor-ferromagnet switch, *Phys. Rev. B* **77**, 184501 (2008).
- [14] S. V. Mironov and A. Buzdin, Standard, inverse, and triplet spin-valve effects in $F_1/S/F_2$ systems, *Phys. Rev. B* **89**, 144505 (2014).
- [15] S. Oh, D. Youm, and M. R. Beasley, A superconductive magnetoresistive memory element using controlled exchange interaction, *Applied Physics Letters* **71**, 2376 (1997).
- [16] M. Božović and Z. Radović, Ferromagnet-superconductor proximity effect: The clean limit, *Europhysics Letters* **70**, 513 (2005).
- [17] K. Halterman and O. T. Valls, Nanoscale ferromagnet-superconductor-ferromagnet switches controlled by magnetization orientation, *Phys. Rev. B* **72**, 060514 (2005).
- [18] V. A. Bobkov, G. A. Bobkov, and I. V. Bobkova, Inverse proximity effect in thin-film superconductor/magnet heterostructures with metallic and insulating magnets (2025), arXiv:2510.18102 [cond-mat.supr-con].
- [19] Y. V. Fominov, A. A. Golubov, T. Y. Karminskaya, M. Y. Kupriyanov, R. G. Deminov, and L. R. Tagirov, Superconducting triplet spin valve, *JETP Letters* **91**, 308 (2010).
- [20] G. Deutscher and F. Meunier, Coupling between ferromagnetic layers through a superconductor, *Phys. Rev. Lett.* **22**, 395 (1969).
- [21] G. Nowak, H. Zabel, K. Westerholt, I. Garifullin, M. Marcellini, A. Liebig, and B. Hjörvarsson, Superconducting spin valves based on epitaxial Fe/V superlattices, *Phys. Rev. B* **78**, 134520 (2008).
- [22] J. Y. Gu, C.-Y. You, J. S. Jiang, J. Pearson, Y. B. Bazaliy, and S. D. Bader, Magnetization-orientation dependence of the superconducting transition temperature in the ferromagnet-superconductor-ferromagnet system: CuNi/Nb/CuNi, *Phys. Rev. Lett.* **89**, 267001 (2002).
- [23] A. Potenza and C. H. Marrows, Superconductor-ferromagnet CuNi/Nb/CuNi trilayers as superconducting spin-valve core structures, *Phys. Rev. B* **71**, 180503 (2005).
- [24] I. C. Moraru, W. P. Pratt, and N. O. Birge, Magnetization-dependent T_c shift in ferromagnet/superconductor/ferromagnet trilayers with a strong ferromagnet, *Phys. Rev. Lett.* **96**, 037004 (2006).
- [25] I. C. Moraru, W. P. Pratt, and N. O. Birge, Observation of standard spin-switch effects in ferromagnet/superconductor/ferromagnet trilayers with a strong ferromagnet, *Phys. Rev. B* **74**, 220507 (2006).
- [26] J. Zhu, I. N. Krivorotov, K. Halterman, and O. T. Valls, Angular dependence of the superconducting transition temperature in ferromagnet-superconductor-ferromagnet trilayers, *Phys. Rev. Lett.* **105**, 207002 (2010).
- [27] A. A. Kamashev, N. N. Garif'yanov, A. A. Validov, V. Kataev, A. S. Osin, Y. V. Fominov, and I. A. Garifullin, Superconducting spin valve effect in Co/Pb/Co heterostructures with insulating interlayers, *Beilstein Journal of Nanotechnology* **15**, 457 (2024).
- [28] Y. Gu, G. B. Halász, J. W. A. Robinson, and M. G. Blamire, Large superconducting spin valve effect and ultrasmall exchange splitting in epitaxial rare-earth-niobium trilayers, *Phys. Rev. Lett.* **115**, 067201 (2015).
- [29] K. Westerholt, D. Sprungmann, H. Zabel, R. Brucas, B. Hjörvarsson, D. A. Tikhonov, and I. A. Garifullin, Superconducting spin valve effect of a v layer coupled to an antiferromagnetic [Fe/V] superlattice, *Phys. Rev. Lett.* **95**, 097003 (2005).
- [30] A. A. Kamashev, N. N. Garif'yanov, A. A. Validov, A. S. Osin, Y. V. Fominov, and I. A. Garifullin, Superconducting spin valve effect in Fe/si₃n₄/Pb/si₃n₄/Fe heterostructures, *Phys. Rev. B* **112**, 134509 (2025).
- [31] S. Bhakat, S. Samanta, S. Mahapatra, and A. Pal, Bistable and absolute switching driven by superconducting exchange coupling, *Nature Communications* **16**, 9609 (2025).
- [32] H. Matsuki, A. Hijano, G. P. Mazur, S. Ilić, B. Wang, I. Alekhina, K. Ohnishi, S. Komori, Y. Li, N. Stelmashenko, N. Banerjee, L. F. Cohen, D. W. McComb, F. S. Bergeret, G. Yang, and J. W. A. Robinson, Realisation of de gennes' absolute superconducting switch with a heavy metal interface, *Nature Communications* **16**, 5674 (2025).
- [33] A. Di Bernardo, S. Komori, G. Livanas, G. Divitini, P. Gentile, M. Cuoco, and J. W. A. Robinson, Nodal superconducting exchange coupling, *Nature Materials* **18**, 1194 (2019).

- [34] T. Kikuta, S. Komori, K. Imura, and T. Taniyama, Electric field enhancement of the superconducting spin-valve effect via strain-transfer across a ferromagnetic/ferroelectric interface, *APL Materials* **12**, 071115 (2024).
- [35] S. Komori, S. Suzuki, K. Imura, and T. Taniyama, Sign control of the critical-temperature switching in oxide superconducting spin valves, *Phys. Rev. Appl.* **23**, L061003 (2025).
- [36] A. Y. Rusanov, S. Habraken, and J. Aarts, Inverse spin switch effects in ferromagnet-superconductor-ferromagnet trilayers with strong ferromagnets, *Phys. Rev. B* **73**, 060505 (2006).
- [37] R. Steiner and P. Ziemann, Magnetic switching of the superconducting transition temperature in layered ferromagnetic/superconducting hybrids: Spin switch versus stray field effects, *Phys. Rev. B* **74**, 094504 (2006).
- [38] A. Singh, C. Sürgers, and H. v. Löhneysen, Superconducting spin switch with perpendicular magnetic anisotropy, *Phys. Rev. B* **75**, 024513 (2007).
- [39] D. H. Kim and T. Hwang, Domain stability effect on magnetoresistance in ferromagnet/superconductor/ferromagnet trilayers, *Physica C: Superconductivity and its Applications* **455**, 58 (2007).
- [40] P. V. Leksin, R. I. Salikhov, I. A. Garifullin, H. Vinzelberg, V. Kataev, R. Klingeler, L. R. Tagirov, and B. Büchner, Observation of the “inverse” spin valve effect in a Ni/V/Ni trilayer system, *JETP Letters* 10.1134/S0021364009130128 (2009).
- [41] J. Zhu, X. Cheng, C. Boone, and I. N. Krivorotov, Origin of the inverse spin switch effect in superconducting spin valves, *Phys. Rev. Lett.* **103**, 027004 (2009).
- [42] N. Banerjee, C. B. Smiet, R. G. J. Smits, A. Ozaeta, F. S. Bergeret, M. G. Blamire, and J. W. A. Robinson, Evidence for spin selectivity of triplet pairs in superconducting spin valves, *Nature Communications* **5**, 3048 (2014).
- [43] F. Colangelo, M. Modestino, F. Avitabile, A. Galluzzi, Z. M. Kakhaki, A. Kumar, J. Linder, M. Polichetti, C. Attanasio, and C. Cirillo, Unveiling intrinsic triplet superconductivity in noncentrosymmetric nbre through inverse spin-valve effects (2025), [arXiv:2510.08110 \[cond-mat.supr-con\]](https://arxiv.org/abs/2510.08110).
- [44] B. Stoddart-Stones, X. Montiel, M. G. Blamire, and J. W. A. Robinson, Competition between the superconducting spin-valve effect and quasiparticle spin-decay in superconducting spin-valves, *Communications Physics* **5**, 224 (2022).
- [45] C.-T. Wu and O. T. Valls, Superconducting proximity effects in ferromagnet/superconductor heterostructures, *Journal of Superconductivity and Novel Magnetism* **25**, 2173 (2012).
- [46] P. V. Leksin, N. N. Garif’yanov, I. A. Garifullin, Y. V. Fominov, J. Schumann, Y. Krupskaya, V. Kataev, O. G. Schmidt, and B. Büchner, Evidence for triplet superconductivity in a superconductor-ferromagnet spin valve, *Phys. Rev. Lett.* **109**, 057005 (2012).
- [47] A. A. Jara, C. Safranski, I. N. Krivorotov, C.-T. Wu, A. N. Mal’nik, O. T. Valls, and K. Halterman, Angular dependence of superconductivity in superconductor/spin-valve heterostructures, *Phys. Rev. B* **89**, 184502 (2014).
- [48] A. Singh, S. Voltan, K. Lahabi, and J. Aarts, Colossal proximity effect in a superconducting triplet spin valve based on the half-metallic ferromagnet CrO_2 , *Phys. Rev. X* **5**, 021019 (2015).
- [49] M. G. Flokstra, T. C. Cunningham, J. Kim, N. Satchell, G. Burnell, P. J. Curran, S. J. Bending, C. J. Kinane, J. F. K. Cooper, S. Langridge, A. Isidori, N. Pugach, M. Eschrig, and S. L. Lee, Controlled suppression of superconductivity by the generation of polarized cooper pairs in spin-valve structures, *Phys. Rev. B* **91**, 060501 (2015).
- [50] T. Y. Karminskaya, A. A. Golubov, and M. Y. Kupriyanov, Anomalous proximity effect in spin-valve superconductor/ferromagnetic metal/ferromagnetic metal structures, *Phys. Rev. B* **84**, 064531 (2011).
- [51] A. A. Kamashev, N. N. Garif’yanov, A. A. Validov, V. Kataev, A. S. Osin, Y. V. Fominov, and I. A. Garifullin, Expanding the operational temperature window of a superconducting spin valve, *Phys. Rev. B* **109**, 144517 (2024).
- [52] A. K. Geim and I. V. Grigorieva, Van der Waals heterostructures, *Nature* **499**, 419 (2013).
- [53] K. S. Novoselov, A. Mishchenko, A. Carvalho, and A. H. Castro Neto, 2D materials and van der Waals heterostructures, *Science* **353**, aac9439 (2016).
- [54] K. Zollner and J. Fabian, Proximity effects, topological states, and correlated physics in graphene heterostructures, *2D Materials* **12**, 013004 (2024).
- [55] M. Gibertini, M. Koperski, A. Morpurgo, and et al., Magnetic 2D materials and heterostructures, *Nat. Nanotechnol.* 10.1038/s41565-019-0438-6 (2019).
- [56] R. Zhang and F. R. Willis, Thickness-dependent Curie temperatures of ultrathin magnetic films: Effect of the range of spin-spin interactions, *Phys. Rev. Lett.* 10.1103/PhysRevLett.86.2665 (2001).
- [57] H. L. Zhuang, P. R. C. Kent, and R. G. Hennig, Strong anisotropy and magnetostriction in the two-dimensional stoner ferromagnet Fe_3GeTe_2 , *Phys. Rev. B* **93**, 134407 (2016).
- [58] S. Liu, X. Yuan, Y.-C. Zou, Y. Sheng, C. Huang, E. Zhang, J. Ling, Y. Liu, W. Wang, C. Zhang, J. Zou, K. Wang, and F. Xiu, Wafer-scale two-dimensional ferromagnetic Fe_3GeTe_2 thin films were grown by molecular beam epitaxy, *npj 2D Materials and Applications* **1** (2017).
- [59] Y. Wang, C. Xian, J. Wang, B. Liu, L. Ling, L. Zhang, L. Cao, Z. Qu, and Y. Xiong, Anisotropic anomalous hall effect in triangular itinerant ferromagnet Fe_3GeTe_2 , *Phys. Rev. B* **96**, 134428 (2017).
- [60] B. Chen, Y. Jinhu, H. Wang, M. Imai, H. Ohta, C. Michioka, K. Yoshimura, and M. Fang, Magnetic properties of layered itinerant electron ferromagnet Fe_3GeTe_2 , *Journal of the Physical Society of Japan* **82**, 124711 (2013).
- [61] Y. Deng, Y. Yu, Y. Song, J. Zhang, N. Z. Wang, Z. Sun, Y. Yi, Y. Z. Wu, S. Wu, J. Zhu, J. Wang, X. H. Chen, and Y. Zhang, Gate-tunable room-temperature ferromagnetism in two-dimensional Fe_3GeTe_2 , *Nature* 10.1038/s41586-018-0626-9 (2018).
- [62] J. Yi, H. Zhuang, Q. Zou, Z. Wu, G. Cao, S. Tang, S. Calder, P. Kent, D. Mandrus, and Z. Gai, Competing antiferromagnetism in a quasi-2d itinerant ferromagnet: Fe_3GeTe_2 , *2D Materials* **4**, 011005 (2016).

- [63] F. Zaiyao, H. Bevin, M. Paul, W. Wenbo, S. Tiancheng, S. Joshua, Y. Wang, X. Di, Z. Xiaoyang, A. May, W. Weida, D. Cobden, J. Chu, and X. Xiaodong, Two-dimensional itinerant ferromagnetism in atomically thin Fe_3GeTe_2 , *Nature materials* **17**, 778 (2018).
- [64] M. Bonilla, S. Kolekar, Y. Ma, H. Coy Diaz, V. Sankar, R. Das, T. Eggers, H. Rodriguez Gutierrez, M.-H. Phan, and M. Batzill, Strong room-temperature ferromagnetism in VSe_2 monolayers on van der Waals substrates, *Nature Nanotechnology* **13** (2018).
- [65] Y. Ma, Y. Dai, M. Guo, C. Niu, Y. Zhu, and B. Huang, Evidence of the existence of magnetism in pristine VX_2 monolayers ($X = \text{S}, \text{Se}$) and their strain-induced tunable magnetic properties, *ACS nano* **6**, 1695 (2012).
- [66] X. Zhang, Q. Lu, W. Liu, W. Niu, J. Sun, J. Cook, M. Vaninger, P. Miceli, D. Singh, S.-W. Lian, T.-R. Chang, X. He, J. Du, L. He, G. Bian, and Y. Xu, Room-temperature intrinsic ferromagnetism in epitaxial CrTe_2 ultrathin films, *Nature Communications* **12**, 2492 (2021).
- [67] R.-Z. Zhang, Y.-Y. Zhang, and S.-X. Du, Thickness-dependent magnetic order and phase transition in V_5S_8 , *Chinese Physics B* **29**, 077504 (2020).
- [68] X. Xi, L. Zhao, Z. Wang, H. Berger, L. Forró, J. Shan, and K. Mak, Strongly enhanced charge-density-wave order in monolayer NbSe_2 , *Nature Nanotechnology* **10**, 765 (2015).
- [69] F. Soto, H. Berger, L. Cabo, C. Carballeira, J. Mosqueira, D. Pavuna, P. Toimil, and F. Vidal, Electric and magnetic characterization of NbSe_2 single crystals: anisotropic superconducting fluctuations above T_c , *arXiv:cond-mat/0607383v2* (2006).
- [70] Y. Saito, Y. Nakamura, M. S. Bahramy, Y. Kohama, J. Ye, Y. Kasahara, Y. Nakagawa, M. Onga, M. Tokunaga, T. Nojima, Y. Yanase, and Y. Iwasa, Superconductivity protected by spin-valley locking in ion-gated MoS_2 , *Nature Physics* **12**, 144 (2016).
- [71] D. Wickramaratne, M. Haim, M. Khodas, and I. I. Mazin, Magnetism-driven unconventional effects in Ising superconductors: Role of proximity, tunneling, and nematicity, *Phys. Rev. B* **104**, L060501 (2021).
- [72] F. Aikebaier, T. T. Heikkilä, and J. L. Lado, Controlling magnetism through ising superconductivity in magnetic van der Waals heterostructures, *Phys. Rev. B* **105**, 054506 (2022).
- [73] G. A. Bobkov, K. A. Bokai, M. M. Otrokov, A. M. Bobkov, and I. V. Bobkova, Gate-controlled proximity effect in superconductor/ferromagnet van der Waals heterostructures, *Phys. Rev. Mater.* **8**, 104801 (2024).
- [74] A. S. Ianovskaia, G. A. Bobkov, A. M. Bobkov, and I. V. Bobkova, Magnetic proximity effect in superconductor/ferromagnet van der Waals heterostructures: Dependence on the number of superconducting monolayers, *Phys. Rev. B* (2024).
- [75] G. A. Bobkov, A. M. Bobkov, and I. V. Bobkova, Spin supercurrent in superconductor/ferromagnet van der Waals heterostructures, *Phys. Rev. B* **110**, 104506 (2024).
- [76] G. A. Bobkov, D. S. Rabinovich, A. M. Bobkov, and I. V. Bobkova, Gate-tunable nonlocal josephson effect through magnetic van der waals bilayers, *Phys. Rev. B* **111**, 024506 (2025).
- [77] J. Jo, P. Yuan, H. Yang, S. Mañas-Valero, J. J. Baldoví, Y. Lu, E. Coronado, F. Casanova, F. Bergeret, M. Gobbi, and L. Hueso, Local control of superconductivity in a $\text{NbSe}_2/\text{CrSBr}$ van der Waals heterostructure, *Nature Communications* **14** (2023).
- [78] D. Jiang, T. Yuan, Y. Wu, X. Wei, G. Mu, Z. An, and W. Li, Strong in-plane magnetic field induced reemergent superconductivity in the van der Waals heterointerface of NbSe_2 and CrCl_3 (2020).
- [79] S. Kezilebieke, M. N. Huda, V. Vaño, M. Aapro, S. Ganguli, O. José Silveira Júnior, S. Głodzik, A. Foster, T. Ojanen, and P. Liljeroth, Topological superconductivity in a van der Waals heterostructure, *Nature* **588**, 424 (2020).
- [80] L. Ai, E. Zhang, J. Yang, X. Xie, Y. Yang, Z. Jia, Y. Zhang, S. Liu, Z. Li, P. Leng, X. Cao, X. Sun, T. Zhang, X. Kou, Z. Han, F. Xiu, and S. Dong, Van der Waals ferromagnetic Josephson junctions, *Nature Communications* **12**, 6580 (2021).
- [81] H. Idzuchi, F. Pientka, K.-F. Huang, K. Harada, Ö. Gül, Y. J. Shin, L. T. Nguyen, N. H. Jo, D. Shindo, R. J. Cava, P. C. Canfield, and P. Kim, Unconventional supercurrent phase in ising superconductor josephson junction with atomically thin magnetic insulator, *Nature Communications* **12**, 5332 (2021).
- [82] A. Buzdin and M. Daumens, Inversion of the proximity effect in hybrid ferromagnet-superconductor-ferromagnet structures, *Europhysics Letters* **64**, 510 (2003).
- [83] S. Tollis, M. Daumens, and A. Buzdin, Inversion of the proximity effect in atomic-scale ferromagnet/superconductor/ferromagnet trilayers, *Phys. Rev. B* **71**, 024510 (2005).
- [84] X. Montiel, D. Gusakova, M. Daumens, and A. Buzdin, Proximity effect in atomic-scaled hybrid superconductor/ferromagnet structures: Crucial role of electron spectra, *Europhysics Letters* **86**, 67002 (2009).
- [85] Z. Devizorova and S. Mironov, Spin-valve effect in superconductor/ferromagnet/ferromagnet and ferromagnet/superconductor/ferromagnet structures of atomic thickness, *Phys. Rev. B* **95**, 144514 (2017).
- [86] Z. Devizorova and S. Mironov, Crossover between standard and inverse spin-valve effect in atomically thin superconductor/half-metal structures, *Phys. Rev. B* **100**, 064519 (2019).
- [87] C. Wang, Y. Xu, and W. Duan, Ising superconductivity and its hidden variants, *Accounts of Materials Research* **2**, 526 (2021).
- [88] X. Xi, H. Berger, L. Forró, J. Shan, and K. F. Mak, Gate tuning of electronic phase transitions in two-dimensional nbse_2 , *Phys. Rev. Lett.* **117**, 106801 (2016).
- [89] H. Matsuoka, S. Kajihara, T. Nomoto, Y. Wang, M. Hirayama, R. Arita, Y. Iwasa, and M. Nakano, Band-driven switching of magnetism in a van der waals magnetic semimetal, *Science Advances* **10**, eadk1415 (2024), <https://www.science.org/doi/pdf/10.1126/sciadv.adk1415>.
- [90] R. P. Kaur, D. F. Agterberg, and M. Sigrist, Helical vortex phase in the noncentrosymmetric CePt_3Si , *Phys. Rev. Lett.* **94**, 137002 (2005).
- [91] A. Akbari and P. Thalmeier, Fermi surface segmentation in the helical state of a Rashba superconductor, *Phys. Rev. Res.* **4**, 023096 (2022).
- [92] X. Zhang and F. Liu, Fulde-Ferrell-Larkin-Ovchinnikov pairing induced by a Weyl nodal line in an Ising superconductor with a high critical field, *Phys. Rev. B* **105**,

- 024505 (2022).
- [93] D. Zhao, L. Debbeler, M. Kühne, S. Fecher, N. Gross, and J. Smet, Evidence of finite-momentum pairing in a centrosymmetric bilayer, *Nature Physics* **19**, 1599 (2023).
 - [94] P. Wan, O. Zheliuk, N. F. Q. Yuan, X. Peng, L. Zhang, M. Liang, U. Zeitler, S. Wiedmann, N. E. Hussey, T. T. M. Palstra, and J. Ye, Orbital Fulde-Ferrell-Larkin-Ovchinnikov state in an Ising superconductor, *Nature* **619**, 46 (2023).
 - [95] Y. Ding, J. He, S. Zhang, H. Zuo, P. Gu, J. Cai, X. Zeng, P. Yan, J. Cai, K. Cao, K. Watanabe, T. Taniguchi, P. Dong, Y. Zhang, Y. Wu, X. Zhou, J. Wang, Y. Chen, Y. Ye, J. Liu, and J. Li, Constructing the Fulde-Ferrell-Larkin-Ovchinnikov state in a CrOCl/NbSe₂ van der Waals heterostructure, *Nano Letters* **24**, 12814 (2024), pMID: 39361493, <https://doi.org/10.1021/acs.nanolett.4c03079>.
 - [96] I. V. Bobkova and A. M. Bobkov, Bistable state in superconductor/ferromagnet heterostructures, *Phys. Rev. B* **89**, 224501 (2014).
 - [97] G. Sarma, On the influence of a uniform exchange field acting on the spins of the conduction electrons in a superconductor, *Journal of Physics and Chemistry of Solids* **24**, 1029 (1963).
 - [98] Y. V. Fominov, N. M. Chtchelkatchev, and A. A. Golubov, Nonmonotonic critical temperature in superconductor/ferromagnet bilayers, *Phys. Rev. B* **66**, 014507 (2002).
 - [99] V. Zdravkov, A. Sidorenko, G. Obermeier, S. Gsell, M. Schreck, C. Müller, S. Horn, R. Tidecks, and L. R. Tagirov, Reentrant superconductivity in Nb/cu_{1-x}ni_x bilayers, *Phys. Rev. Lett.* **97**, 057004 (2006).
 - [100] V. I. Zdravkov, J. Kehrle, G. Obermeier, S. Gsell, M. Schreck, C. Müller, H.-A. Krug von Nidda, J. Lindner, J. Moosburger-Will, E. Nold, R. Morari, V. V. Ryazanov, A. S. Sidorenko, S. Horn, R. Tidecks, and L. R. Tagirov, Reentrant superconductivity in superconductor/ferromagnetic-alloy bilayers, *Phys. Rev. B* **82**, 054517 (2010).
 - [101] I. V. Bobkova and A. M. Bobkov, Thermospin effects in superconducting heterostructures, *Phys. Rev. B* **96**, 104515 (2017).